ROYAL SOCIETY
OF CHEMISTRY

PAPER

Preparation and gas transport properties of triptycene-containing polybenzoxazole (PBO)-based polymers derived from thermal rearrangement (TR) and thermal cyclodehydration (TC) processes†

Shuangjiang Luo,[a] Junyi Liu,[b] Haiqing Lin,[b] Barbara A. Kazanowska,[a] Michael D. Hunckler,[c] Ryan K. Roeder[c] and Ruilan Guo*[a]

Polybenzoxazoles (PBOs), such as thermally rearranged (TR) polymers, have been shown to have excellent gas separation performance. Herein we report the preparation and transport properties of two new series of PBO-based polymers that were thermally derived from triptycene-containing *o*-hydroxy polyimide and polyamide precursors *via* a thermal rearrangement (TR) process and a thermal cyclodehydration (TC) process, respectively. Incorporation of triptycene units into poly(hydroxyimide) precursor structures led to a significant increase of fractional free volume and created ultrafine microporosity in the converted PBO-based TR polymers, which enabled both high gas permeabilities and high selectivities. Although the TC process of the poly(hydroxyamide) precursor led to moderate improvement in the separation performance of the resulting triptycene-containing PBO polymers as compared to the TR process, the PBO films converted *via* the TC process exhibited excellent mechanical properties superior to many other TR polymers previously reported in the literature as well as the triptycene-containing TR polymers in this study. In particular, the PBO film thermally rearranged at 450 °C showed a H_2 pure gas permeability of 810 barrer, a CO_2 permeability of 270 barrer, and CO_2/CH_4 and H_2/CH_4 selectivities of 67 and 200, respectively, at 35 °C and 11 atm, which are far beyond the upper bound limits.

1. Introduction

Membrane-mediated gas separation represents an attractive and fast-growing separation technology, due to its advantages of a small footprint, high energy efficiency, low cost and ease of operation and maintenance.[1–3] Producing robust polymeric membranes with both high permeability and high selectivity that defy the permeability-selectivity tradeoff limit, *i.e.*, Robeson's upper bounds,[4,5] has been the main research focus in the field of membrane science and technology. Among the many new membranes reported recently, polymers of intrinsic microporosity (PIMs)[6–10] having stiff ladder-type backbones with contorted sites and thermally rearranged (TR)[11–17] polymers

*a*Department of Chemical and Biomolecular Engineering, University of Notre Dame, Notre Dame, IN 46556, USA. E-mail: rguo@nd.edu; Fax: +1-574-631-8366; Tel: +1-574-631-3453

*b*Department of Chemical and Biological Engineering, University of Buffalo, The State University of New York, Buffalo, NY 14260, USA

*c*Department of Aerospace and Mechanical Engineering, University of Notre Dame, Notre Dame, IN 46556, USA

† Electronic supplementary information (ESI) available: DSC curves of the TPHA-TC films, pictures of PBO films and the feed pressure dependence of pure gas permeabilities. See DOI: 10.1039/c6ta03951k
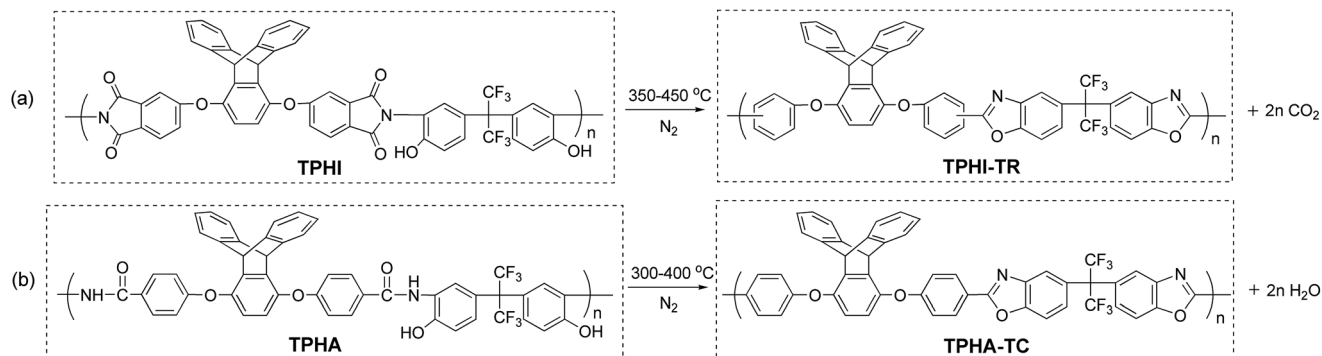
derived from poly(hydroxyimide) precursors are two representative classes of novel separation membrane materials, which display unprecedentedly high gas permeabilities and good selectivities due to highly rigid and contorted backbone structures and high microporosity in the polymers. In particular, TR polymers have polybenzoxazole (PBO)-based structures that are in general fabricated *via* a solid-state thermal rearrangement reaction of poly(hydroxyimide) precursors at high temperatures (usually above 400 °C). The formation of a large amount of microcavities with narrow cavity size distribution upon the TR conversion process is responsible for the extraordinary size-sieving based separation performance of TR polymers.[11] However, TR polymers usually suffer from insufficient mechanical properties most likely due to undesired thermal degradation at high temperature treatment, which also partially explains the much less attractive gas selectivities of TR polymers considering their ultra-high gas permeabilities. To address this issue, a variety of TR-based copolymers have been prepared and studied, which include copolymers with non-rearrangable polyimide,[18] polypyrrolone,[19] and poly(aromatic ether).[20] However, most of these PBO-based copolymers are not comparable in their separation performance to the earlier TR polymers despite their improved mechanical properties. Thermal

17050 | *J. Mater. Chem. A*, 2016, **4**, 17050–17062

This journal is © The Royal Society of Chemistry 2016

Scheme 1 (a) Thermal rearrangement (TR) of the triptycene-containing TPHI poly(hydroxyimide) precursor and (b) thermal cyclodehydration (TC) of the triptycene-containing TPHA poly(hydroxyamide) precursor to form PBOs.

cyclodehydration (TC) of poly(hydroxyamide) precursors has been reported as an alternative low-temperature approach to produce PBO polymers similar to TR polymers. The TC process involves solid-state cyclodehydration reactions at temperatures that are typically about 100 °C lower than the TR conversion temperature to achieve full PBO conversion.[16,21–24] As such, PBO polymers prepared *via* the TC process are much mechanically stronger than those converted *via* the TR process due to the elimination of thermal degradation.[16] On the other side, due to less significant changes in chain conformations during the TC conversion process, PBO polymers converted from poly-(hydroxyamide) precursors *via* the TC process are generally less permeable than the TR polymers with similar structures. Based on the abovementioned studies, it is clear that new poly-(hydroxyimide) and poly(hydroxyamide) precursor structures are still highly demanded so that mechanically robust PBO-based gas separation membranes can be produced in a more efficient way (*i.e.*, low conversion temperature) that possess exceptionally high permeability–selectivity combinations.[11–17]

Recently, microporous polymers containing iptycene units in the backbone structures were developed and studied as gas separation membranes, which showed very promising gas separation performance.[9,10,12,25–32] Iptycenes, *e.g.*, triptycene and pentiptycene, are a large family of molecules containing multiple arene rings fused together into three-dimensional, bulky structures.[33,34] When incorporated into polymer backbone structures, the bulky iptycene units efficiently disrupt chain packing, resulting in a large fractional free volume and consequently, greatly enhanced gas permeability.[9,10,12,25–31] More importantly, we have demonstrated that the so-called internal free volume defined as the open clefts between the benzene "blades" not only introduces a significant amount of molecular cavities enabling high gas permeabilities, but also the size of these internal molecular cavities is comparable with the kinetic diameters of important gas molecules (*e.g.*, H_2, CO_2, O_2, N_2, and CH_4) relevant to industrial separations, which provides an efficient approach to finely tune the overall microcavity size and size distribution, affording high gas selectivities *via* precise size sieving.[26–28]

In this study, we seek a novel combination of PBO-based TR polymers and iptycene structural units, whereby superior gas permeabilities of TR polymers are synergistically integrated with the ultrafine microporosity induced by iptycene-based structures leading to significantly improved selectivities in the resulting TR polymers. In particular, we report in this paper the synthesis and characterization of two new triptycene-containing poly(hydroxyimide) and poly(hydroxyamide) precursors, *i.e.*, TPHI and TPHA, which are prepared from commercial 2,2′-bis(3-amino-4-hydroxyphenyl)hexafluoropropane (6FAP) and custom-synthesized triptycene-containing dianhydride or di(acid chloride) monomer. Systematic studies of the solid-state thermal rearrangement and thermal cyclodehydration reactions (Scheme 1) using the triptycene-containing precursors are presented and the PBO conversion efficiency is analyzed as a function of thermal treatment temperature for both TR and TC processes. Comprehensive characterization and analysis of physical properties in terms of fractional free volume, polymer chain packing, mechanical properties and pure-gas transport properties of the resulting triptycene-containing PBO films are also provided to establish the fundamental structure–property relationships for these new PBO-based polymers.

2.　Experimental

2.1.　Materials

2,2′-Bis(3-amino-4-hydroxyphenyl)hexafluoropropane (6FAP, >98.5%) was purchased from Akron Polymer Systems and dried at 65 °C in a vacuum oven overnight prior to use. 4-Nitrobenzonitrile (97%), thionyl chloride (≥99%), chlorotrimethylsilane (TMCS, ≥99%), anhydrous pyridine (≥99.8%) and anhydrous *N*-methyl-2-pyrrolidone (NMP, ≥98%) were purchased from Sigma-Aldrich and used as received. All other chemicals were obtained from commercial sources and used as received.

2.2.　Synthesis of the triptycene-containing diacid chloride (TPDC) monomer

The triptycene-containing diacid chloride (TPDC) monomer was synthesized *via* a chloroformylation reaction of an intermediate triptycene diacid which was prepared *via* hydrolysis of the triptycene dinitrile compound, as shown in Scheme 2. The
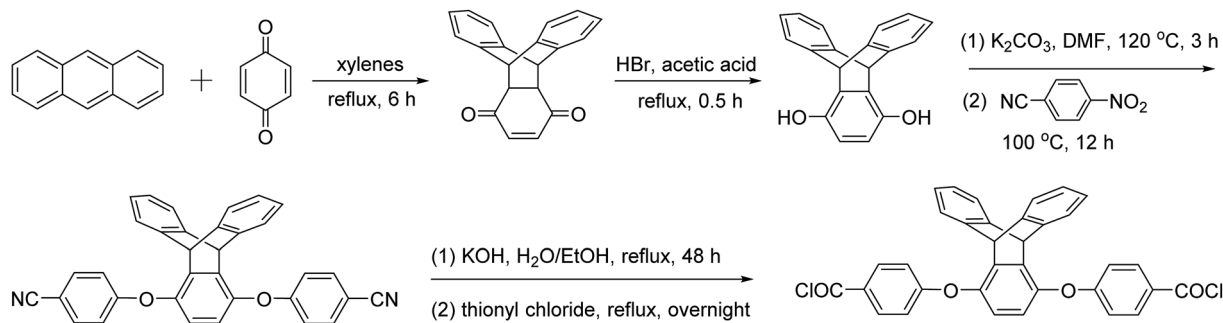
Scheme 2 Synthesis of the triptycene-containing diacid chloride monomer (TPDC).

triptycene dinitrile compound was synthesized as follows: a mixture of triptycene 1,4-hydroquinone[28,35] (4.30 g, 15 mmol), anhydrous potassium carbonate (4.25 g, 31 mmol), dimethylformamide (DMF, 45 mL) and toluene (9 mL) was charged into a two-neck flask equipped with a Dean–Stark trap and a nitrogen inlet. The mixture was stirred and refluxed at 120 °C under a nitrogen atmosphere for 3 h, during which water was removed as an azeotrope with toluene. The reaction was then cooled down to room temperature and 4-nitrobenzonitrile (4.70 g, 31 mmol) was added. After reacting at 100 °C overnight, the mixture was precipitated in a water/methanol (v/v = 5/1, 400 mL) mixture. The solid was filtered and washed repeatedly with water and methanol, and then dried at 120 °C under vacuum to afford white powder as triptycene dinitrile (7.58 g, yield 85%). ^{1}H NMR (500 MHz, CDCl$_3$): δ 5.49 (s, 2H), 6.76 (s, 2H), 6.89–6.91 (d, J = 8.75 Hz, 4H), 7.00–7.02 (m, 4H), 7.18–7.20 (m, 4H), 7.61–7.63 (d, J = 8.75 Hz, 4H). ATR-FTIR (ν, cm^{-1}): 2234 (C≡N str).

Hydrolysis and chloroformylation of triptycene dinitrile were conducted as follows: to a one-neck flask was added a suspension of the triptycene dinitrile compound (5.0 g, 10 mmol) in an ethanol/water mixture (50 mL/50 mL) containing 20 g of potassium hydroxide (KOH, 0.356 mol), and the mixture was refluxed for 48 h. After cooling to room temperature, the resulting clear solution was acidized to pH = 1.0 with concentrated HCl solution and formed precipitates of triptycene dicarboxylic acid, which were collected *via* filtration and washed repeatedly with deionized (DI) water. After drying in a vacuum oven at 120 °C overnight, the obtained triptycene dicarboxylic acid was refluxed in thionyl chloride (20 mL) overnight. The pale-yellow powder product was collected by evaporating residual thionyl chloride and vacuum drying at 65 °C overnight as triptycene diacid chloride (TPDC, 5.13 g, yield 96%). ^{1}H NMR (500 MHz, CDCl$_3$): δ 5.52 (s, 2H), 6.80 (s, 2H), 6.91–6.93 (m, 4H), 7.00–7.03 (m, 4H), 7.19–7.21 (m, 4H), 8.10–8.12 (m, 4H).

2.3. Synthesis of the triptycene-containing poly(hydroxyamide) precursor (TPHA)

The TPHA poly(hydroxyamide) precursor was synthesized by condensation polymerization between TPDC and 6FAP using the silylation method reported earlier (Scheme 3).[16,36,37] 6FAP (1.4006 g, 3.8 mmol) and anhydrous NMP (14 mL) were added into a flame-dried, three-neck flask equipped with a mechanical

stirrer and a nitrogen inlet. After the complete dissolution of 6FAP, TMCS (2.3 mL, 18.4 mmol) and pyridine (1.6 mL, 19.4 mmol) were added, and the mixture was stirred at room temperature for 2 h to complete the silylation of 6FAP. The flask was then immersed in an ice-water bath followed by addition of TPDC (2.1765 g, 3.8 mmol) and anhydrous pyridine (0.8 mL, 9.7 mmol). The solution was stirred in the ice-water bath for 2 h after which the temperature was gradually increased to room temperature. The condensation polymerization continued at room temperature overnight to form a viscous solution of silylated polyamide. The resulting polymer solution was precipitated in 1 : 1 methanol/water mixture (v/v, 600 mL) and then washed thoroughly with fresh methanol to hydrolyze the silylated groups to final hydroxyl groups. The fibrous polymer product was collected and dried at 180 °C under vacuum overnight affording a white solid as TPDC-6FAP-TPHA (3.38 g, yield 98%). ^{1}H NMR (500 MHz, DMSO-d_6): δ 5.70 (s, 2H), 6.85 (s, 2H), 6.96 (s, 2H), 6.97 (s, 2H), 6.97–6.98 (m, 4H), 6.98–6.99 (m, 4H), 7.26–7.28 (m, 4H), 7.96 (s, 4H), 7.98 (s, 2H), 9.48 (s, 2H), 10.37 (s, 2H). ATR-FTIR (membrane, ν, cm^{-1}): ∼3300 (br, –OH), 1648 (amide C=O str), 1536 (amide C–N str). Molecular weight measured by size exclusion chromatography (SEC), (DMF eluent, polystyrene standards): M_n = 2.42 × 10^4 g mol^{-1}, M_w = 8.04 × 10^4 g mol^{-1}, PDI = 3.31.

2.4. Synthesis of the triptycene-containing poly(hydroxyimide) precursor (TPHI)

The triptycene-containing poly(hydroxyimide) precursor, TPHI, was synthesized *via* solution thermal imidization as described in our previous study.[27] Poly(amic acid) was first formed by the reaction between triptycene-containing dianhydride (TPDAn) and 6FAP, and it was then converted to polyimide through solution thermal imidization using *o*-dichlorobenzene as an azeotropic reagent at 190 °C overnight. Isotropic films were obtained by a solution casting method and the films were further thermally treated in a Thermo-Scientific muffle furnace at 300 °C under a nitrogen atmosphere for 2 h to afford a fully imidized TPHI polyimide thin film.

2.5. Film formation and thermal conversion

The fibrous TPDC-6FAP-TPHA precursor was dissolved in NMP to form a clear polymer solution (∼5% w/v, g mL^{-1}), which was
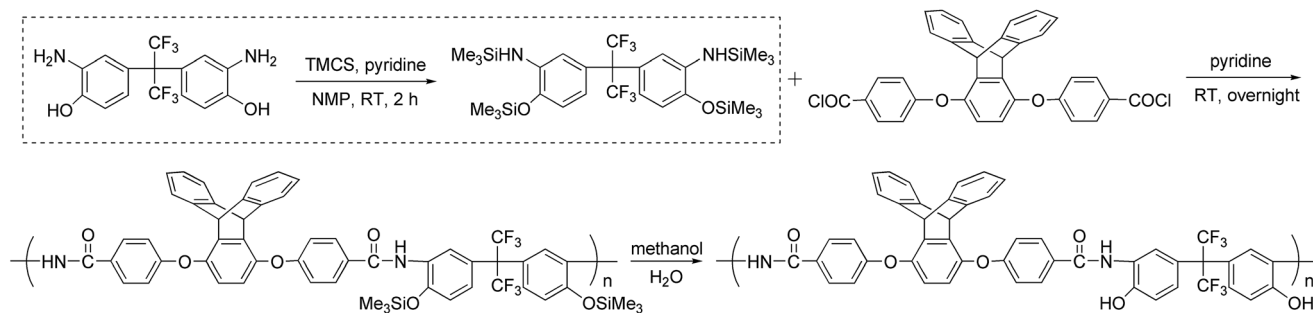
Scheme 3 Synthesis of the triptycene–containing poly(hydroxyamide) precursor.

cast onto a clean, leveled glass plate after being filtered with a 0.45 μm Teflon syringe filter. The glass plate with cast polymer solution was placed under an infra-red lamp (Staco Energy Products Co., 120 V) overnight to slowly evaporate the solvent at around 60 °C, after which it was further dried in a vacuum oven at 180 °C overnight. The resulting film was teared off from the plate and soaked in fresh methanol for 24 h to extract the remaining casting solvent. The final drying of the polymer films was conducted at 180 °C overnight under vacuum to completely remove the residual solvent. Thin films of the TPDAn-6FAP-TPHI precursor were prepared according to our previous report.[27] The film thickness (30–70 μm) was measured using a digital micrometer, and the effective area of the polymer films for the gas permeation test was determined using a digital scanner (LiDE120, Canon) by analyzing the scanned images with ImageJ software.

Both TPHI and TPHA precursor films were thermally converted to corresponding TPHI-TR and TPHA-TC PBOs at predetermined temperatures for a controlled amount of time in a furnace under nitrogen protection. Experimentally, the precursor films were cut into ∼5 × 5 cm pieces and sandwiched between two porous ceramic plates before they were thermally treated in a preheated Thermo-Scientific muffle furnace under an ultrahigh-purity nitrogen atmosphere. After the films were heated at a desired temperature for a predetermined amount of time, the furnace was cooled down to room temperature at a cooling rate no greater than 10 °C min⁻¹. In particular, TPHI precursor films were heated at 350 and 400 °C for 2 h, and 450 °C for 30 minutes, and the resulting films were referred to as TPHI-TR-350, TPHI-TR-400 and TPHI-TR-450, respectively. Similarly, TPHA precursor films were treated at 300 and 350 °C for 2 h, and 400 °C for 1 h, affording TPHA-TC-300, TPHA-TC-350 and TPHA-TC-400, respectively.

2.6. Characterization methods

^{1}H NMR spectra were recorded on a Bruker AVANCE III HD 500 spectrometer using deuterated chloroform (CDCl₃) or deuterated dimethylsulfone (DMSO-d_6) as the solvent. Fourier transform infrared (ATR-FTIR) spectra of the polymers were recorded on a JASCO FT-IR 6300 spectrometer in attenuated total reflection (ATR) mode with a resolution of 4 cm⁻¹ and 64 scans. Molecular weight and molecular weight distribution of the polyamide precursor were measured using a size exclusion chromatograph (SEC, Waters GPC System), which was equipped with a Waters 515 HPLC pump, three Polymer Standards Service (PSS) columns (GRAM, 10^4, 10^3, and 10^2 Å) with a DMF flow rate of 1 mL min⁻¹ at 55 °C, and a Waters 2414 refractive index detector connected to PSS WinGPC 7.5 software. Polystyrene was used as an external standard and DMF as the eluent.

Thermo-gravimetric analysis (TGA) was performed on a TGA Q500 (TA Instruments) at a heating rate of 10 °C min⁻¹ with a nitrogen purge of 50 mL min⁻¹. Differential scanning calorimetry (DSC) analyses were carried out under nitrogen purge (50 mL min⁻¹) on a DSC Q2000 (TA Instruments) at a heating rate of 10 °C min⁻¹ and cooling rate of 20 °C min⁻¹. Two heating cycles were applied with the highest temperature in the first heating cycle below the PBO conversion temperature and the second heating cycle in the range of 100–400 °C. Glass transition temperature (T_g) and thermal conversion temperature were determined based on the second heating profile using the automatic mode of TA Universal Analysis software.

Wide-angle X-ray diffraction (WAXD) patterns of the polymers were recorded in the reflection mode at room temperature on a Bruker D8 Advance Davinci diffractometer with Cu Kα radiation (wavelength λ = 1.54 Å) operating at 40 mA and 40 kV. The scan speed and step size were 5 seconds per step and 0.02° per step, respectively, and the average d-spacing values were calculated using Bragg's law in the 2θ range of 5–45°.

Mechanical properties of the polymer films were tested in uniaxial tension at room temperature following ASTM D882-12.[38] The as-prepared films, 40–70 μm in thickness with less than 10% variation along the gauge length, were cut into strips 5 mm in width. Specimens were clamped using flat knurled grips with a thin rubber facing (<75 μm thickness). The specimen gauge length was 22 mm, instead of the 100 mm specified in ASTM D882-12, due to size constraints of the as-prepared membranes. All specimens were loaded to failure in uniaxial tension at a displacement rate of 2.2 mm min⁻¹ using a Bose ElectroForce 3300 electromechanical test instrument. The elastic modulus, tensile strength, and percent elongation at break were calculated from force–displacement data and reported as the mean ± standard deviation for at least five specimens per group.

Densities of the polymers were measured in the thin film state by means of the buoyancy method using an analytical balance (ML204, Mettler Toledo) equipped with a density kit in

This journal is © The Royal Society of Chemistry 2016

J. Mater. Chem. A, 2016, **4**, 17050–17062 | **17053**

deionized (DI) water at room temperature. Correspondingly, the fractional free volume (FFV) was calculated as follows:

$$\text{FFV} = \frac{V_0 - 1.3V_w}{V_0} \qquad (1)$$

where V_0 is the molar volume of the polymer derived from the density measurement, and V_w is the van der Waals volume obtained from Bondi's group contribution method.[39,40] The V_w values of the partially converted polymers were estimated via $V_w = x_1 V_{w_1} + x_2 V_{w_2}$, where x_1 and x_2 are the molar fractions of the precursor and PBO, respectively, which were determined by comparing the weight loss during the thermal treatment to that of the theoretical weight loss at full conversion; V_{w_1} and V_{w_2} are the respective van der Waals volume for the two constituents.

Pure gas permeabilities (P) of four gases (i.e., H_2, CH_4, N_2, and CO_2) were tested at 35 °C using the constant-volume/variable-pressure method.[41] After the films were degassed on both sides overnight, ultra-high purity grade gases were introduced in the upstream and maintained at a certain pressure (i.e., 4.4, 7.8, 11.2 or 14.6 atm), while the steady state pressure increase as a function of time in the downstream was recorded as the permeation rate, which was used to calculate the permeability coefficient as follows:

$$P = 10^{10} \frac{V_d l}{p_{up} TRA} \left[\left(\frac{dp}{dt} \right)_{ss} - \left(\frac{dp}{dt} \right)_{leak} \right] \qquad (2)$$

where P (barrer, 1 barrer = 10^{-10} cm^3 (STP) cm per cm^2 s cmHg) is the gas permeability coefficient, V_d is the downstream volume (cm^3), l is the membrane thickness (cm), p_{up} is the upstream pressure (cmHg), T is the temperature (K), R is the gas constant (0.278 cm^3 cmHg per cm^3 (STP) K), A is the effective area (cm^2), dp/dt is the steady-state pressure increment in downstream (cmHg per s) and $(dp/dt)_{leak}$ is the leak rate of the system (cmHg per s). The ideal selectivity ($\alpha_{A/B}$) of one gas pair (A and B) was defined as the ratio of pure gas permeability of the two gases:

$$\alpha_{A/B} \equiv \frac{P_A}{P_B} \qquad (3)$$

3.   Results and discussion

3.1.   Synthesis of triptycene-containing TPHI and TPHA precursors

Two types of triptycene-containing PBO precursors with ortho-positioned hydroxyl groups, i.e., poly(hydroxyimide) (TPHI) and poly(hydroxyamide) (TPHA), were prepared in this study to investigate how different PBO formation mechanisms, i.e., thermal rearrangement (TR) of TPHI and thermal cyclo-dehydration (TC) of TPHA (Scheme 1), influence the microstructure and consequent transport properties of the resulting PBO-based polymers. In particular, the triptycene-containing TPHI precursor was synthesized from a previously reported triptycene-based dianhydride (TPDAn) and a hydroxyl-containing aromatic diamine (6FAP) via conventional solution thermal imidization, and the fully imidized structure with ortho-hydroxyl groups was confirmed by ^{1}H NMR.[27] To synthesize the

TPHA precursor, a new triptycene-based diacid chloride monomer (TPDC) was first synthesized via chloroformylation of the intermediate dicarboxylic acid compound (Scheme 2). The monomer was obtained with high yield (>83%) and high purity was confirmed by ^{1}H NMR (Fig. 1a). Condensation polymerization between TPDC and 6FAP using the silylation method produced the triptycene-containing TPHA precursor (Scheme 3). The silylation method was adopted because it has been shown to be able to produce linear, high molecular weight polyamides by avoiding undesired side reactions involving ortho-hydroxyl groups.[16,36,37] The presence of the characteristic bridgehead proton of triptycene (peak c), hydroxyl proton (–OH) and amide bond proton (–NH) as well as the absence of the trimethylsilane protons in the ^{1}H NMR spectrum (Fig. 1b) confirmed the anticipated structure of TPHA and complete hydrolysis of trimethylsilane groups after precipitation and washing with methanol. The obtained TPHA showed a high molecular weight (>2.4 × 10^4 g mol^{-1}), indicating good reactivity of TPDC and 6FAP towards the polycondensation reaction. Transparent, flexible thin films were obtained through a conventional solution casting method using NMP as the casting solvent.

3.2.   Thermal conversion of TPHI and TPHA precursor films

Thermal rearrangement (TR) of an aromatic poly(hydroxyimide) precursor, such as TPHI in this study, involves the reaction between the ortho-hydroxyl groups and either of the adjacent imide carbonyl groups under thermal treatment in an inert atmosphere, producing a mixture of meta/para linked PBO structures (Scheme 1a).[11,13,14,42–46] The TR process of poly(hydroxyimide) precursors can be feasibly tracked by thermogravimetric analyses, from which TGA profiles featuring two-stage weight losses are typically observed. In this study, a TGA temperature ramp was conducted to evaluate the TR process of the TPDAn-6FAP-TPHI precursor as well as to establish suitable
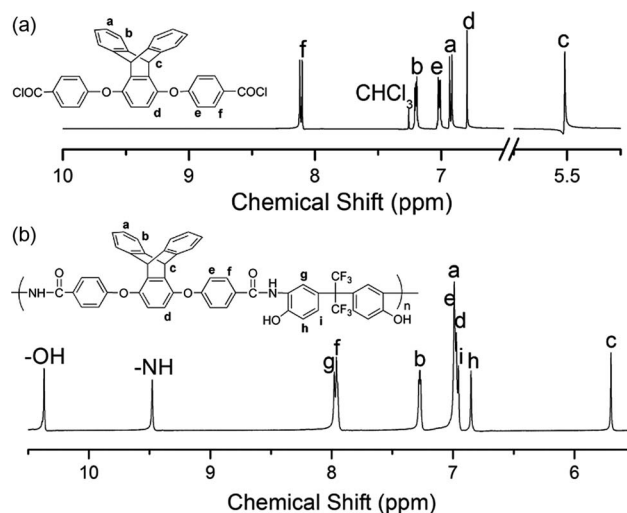

Fig. 1 ^{1}H NMR spectra of the (a) triptycene-based diacid chloride monomer (CDCl$_3$, 500 MHz) and (b) triptycene-containing poly(hydroxylamine) TPHA precursor (DMSO-d_6, 500 MHz).

17054 | J. Mater. Chem. A, 2016, 4, 17050–17062

This journal is © The Royal Society of Chemistry 2016

thermal treatment protocols. As shown in Fig. 2a, a clear two-stage weight loss TGA profile was observed, suggesting that thermal rearrangement occurred in the TPHI precursor. Moreover, weight loss of the first stage matches well with the theoretical value (9.7%) of the TR decarboxylation process (*i.e.*, release of two CO_2 molecules per repeat unit),[20,42,47–52] which further confirms the conversion to PBO structures upon thermal treatment. Similarly, the TPDC-6FAP-based TPHA precursor also exhibits a two-stage weight loss TGA profile, and the observed weight loss of the first stage corresponds well with the theoretical weight loss (4.2%) of cyclodehydration (*i.e.*, release of two H_2O molecules per repeat unit),[22,24,53] suggesting the occurrence of PHA-to-PBO conversion. In both cases, the second weight loss is ascribed to the thermal degradation of PBOs that were formed during the TR or TC process. Both the starting degradation temperature (~500 °C) and the weight loss (~30%) during the degradation of the PBOs are almost the same for TR and TC processes, indicating that similar PBO structures were formed during both solid-state reactions. It should be mentioned that triptycene moieties are highly thermally stable during thermal treatments as evidenced by the very high thermal degradation temperature ($T_{d,5\%}$ > 518 °C) demonstrated in several of our previously reported triptycene-containing polyimides,[27,28] which have similar structures to TPHI and TPHA precursors. As such, the first-stage weight loss observed in the TGA profiles of TPHI and TPHA precursors is exclusively ascribed to the conversion of precursors to PBOs and triptycene moieties remained intact upon solid-state thermal treatment.

Compared to the TR process of the TPHI precursor, the starting temperature for the TC process of the TPHA precursor is around 80 °C lower, and the cyclodehydration conversion temperature range (270–360 °C) is much narrower than that of the TR process (350–490 °C). This observation is consistent with our previous report that thermal cyclodehydration of poly(hydroxyamide) precursors (*e.g.*, TPHA) is a more feasible and efficient approach to obtain PBO structures than the TR process

of poly(hydroxyimide) precursors (*e.g.*, TPHI).[16] Previous studies have also demonstrated that TR conversion temperature is strongly dependent on the T_g of the poly(hydroxyimide) precursors, and the TR process usually has to be conducted above the T_g of the precursors to affect molecular rearrangement reactions.[13,15,42] On the other hand, the thermal cyclodehydration of poly(hydroxyamide) precursors was found to be relatively independent of the glass transition temperature of the precursors due to different reaction mechanisms.[16] DSC analyses of both TPHI and TPHA precursors were conducted and the DSC thermograms (*i.e.*, the second heating curves) are shown in Fig. S1 in the ESI.† As shown, the TPHI precursor exhibited a T_g of ~305 °C and no obvious endothermic event associated with the TR process was observed up to nearly 400 °C. On the other hand, TPHA precursor displayed a broad endothermic cyclodehydration peak, which might overlap with the T_g of TPHA. Moreover, the temperature range (~270–360 °C) of the endothermic peak observed in DSC curves agrees with that observed in the TGA weight loss derivative curves. The DSC results further confirmed that cyclodehydration of poly(hydroxyamide) precursors can take place at or even slightly below the T_g of the precursors, and the lower thermal conversion temperature of TPHA can be ascribed to the lower activation energy barrier for hydroxyamide-to-benzoxazole conversion than that of hydroxyimide-to-benzoxazole conversion.[16,47]

The evolutionary structural changes from imide or amide structures to benzoxazole structures upon thermal treatments were monitored by ATR-FTIR by tracking the disappearance of characteristic bands of the precursors and the appearance of benzoxazole characteristic bands of the resulting PBO-based polymers. As shown in Fig. 3a, the characteristic imide bands (1782 cm^{-1}, C=O; 1105 cm^{-1}, C–N–C) of the TPHI precursor are still present even after the film was thermally treated at 450 °C, suggesting incomplete TPHI-to-PBO conversion. Similar observations were reported for other poly(hydroxyimide) precursors,
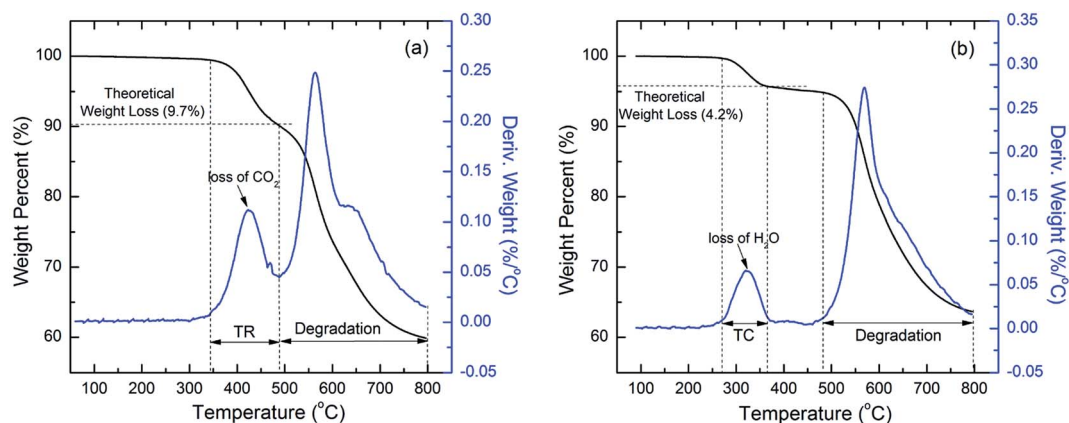

Fig. 2 TGA weight loss and weight loss derivative curves of the (a) TPDAn-6FAP-TPHI precursor and (b) TPDC-6FAP-TPHA precursor. The horizontal dashed lines denote the theoretically predicted weight loss upon full PBO conversion in the thermal rearrangement and thermal cyclodehydration reactions. Regions of thermal rearrangement (TR), thermal cyclodehydration and degradation are separated by vertical dashed lines.
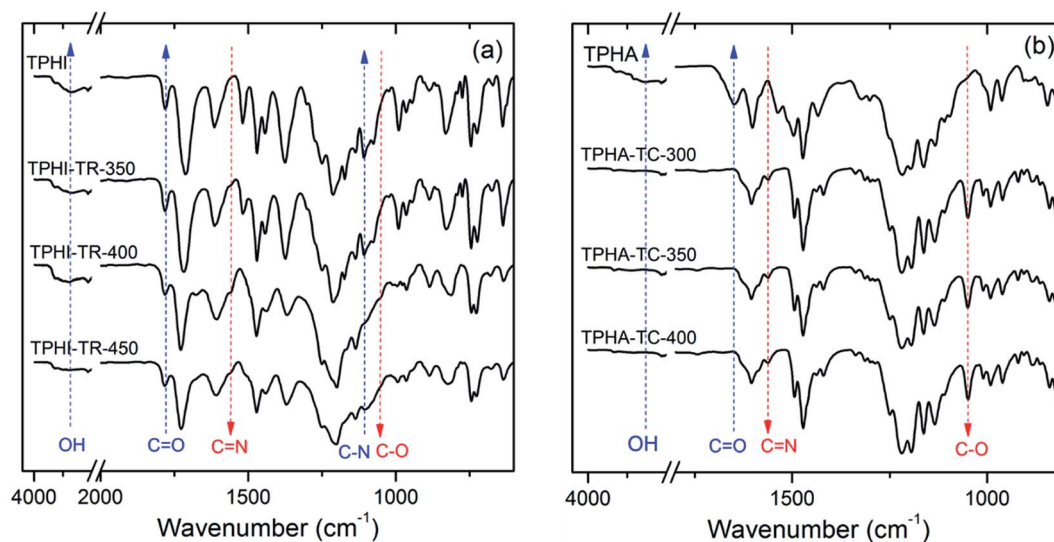
This journal is © The Royal Society of Chemistry 2016

J. Mater. Chem. A, 2016, **4**, 17050–17062 | **17055**

Fig. 3 ATR–FTIR spectra of (a) thermal rearrangement of TPHI and (b) thermal cyclodehydration of TPHA at different temperatures. The arrows in the spectra indicate the decrease or increase in the intensity of specific characteristic bands.

where incomplete conversion and weak PBO absorbance bands were observed.[13,16,21,47,48,51] On the other hand, the characteristic hydroxyl group (~3300 cm⁻¹) and the amide bond (1650 cm⁻¹, C=O) of the TPHA precursor disappeared, and distinct PBO characteristic bands (1562 cm⁻¹, C=N; 1048 cm⁻¹, C–O) appeared after the TPHA precursor was thermally treated at 300 °C. Additionally, TPHA films treated at higher temperatures (i.e., 350 and 400 °C) exhibit almost identical FTIR spectra, confirming that complete TPHA-to-PBO conversion was achieved under thermal treatment at 300 °C for 2 h. FTIR results are consistent with the TGA and DSC results, which indicates that the TPHA-to-PBO cyclodehydration conversion is more favorable and efficient than the TR process of TPHI-to-PBO conversion.

The degree of PBO conversion as a function of treatment temperature was quantitatively estimated using a gravimetric method by taking the ratio of experimentally observed weight loss to the theoretically predicted weight loss, and the results are listed in Table 1. As expected, the degree of PBO conversion generally increases with increasing treatment temperature for the TPHI-TR series, and the experimental weight loss of TPHI-TR-450 is higher than the theoretical value possibly due to thermal degradation. For simplicity, full conversion is assumed when the measured weight loss of a sample is greater than the predicted value and the excess weight loss is treated as the fraction of degradation. For the TPHA-series, complete conversion to PBO structures was readily reached at all three treatment temperatures (i.e., 300, 350 and 400 °C). The completion of TPHA-to-PBO conversion was also confirmed with DSC thermograms (Fig. S1b†), in which the cyclodehydration peak of the TPHA precursor diminished in all treated films and high glass transition temperatures (>300 °C) were observed for the converted films, suggesting the formation of highly rigid PBO structures. Among the converted TPHA-TC films, the T_g of the converted films increased with the increment of thermal cyclodehydration temperature, which is probably due to the increased tendency towards thermal inter-chain cross-linking at high temperatures.[13,21,22] Although thermal degradation was observed for all converted TPHA-TC films, it should be noted that the degradation is much less significant than in the case of TPHI-TR films.

Table 1 Degree of PBO conversion of the thermally treated polymer thin films obtained at different temperatures

Thermal treatment temperature (°C)	TPDAn-6FAP-TPHI			TPDC-6FAP-TPHA		
	Weight loss observed (%)	PBO conversion[a] (%)	Fraction of degradation[b] (%)	Weight loss observed (%)	PBO conversion[a] (%)	Fraction of degradation[b] (%)
Precursor	—	—	—	—	—	—
300	—	—	—	5.7	100[c]	1.5
350	2.7	28	—	6.3	100[c]	2.1
400	8.4	87	—	7.0	100[c]	2.8
450	14.2	100[c]	4.5	—	—	—

[a] Theoretical weight losses for TPHI and TPHA precursors are 9.7% and 4.2%, respectively. [b] Degree of degradation was estimated as the excess weight loss compared to theoretical values. [c] Full conversion to PBO was assumed when measured weight loss was greater than theoretical weight loss.

3.3. Membrane properties of the precursor films and converted films

The formation of PBO structures via both TR and TC processes is accompanied by significant changes of chain conformation and chain packing, which certainly induce dramatic changes in the fractional free volume (FFV) and consequent gas transport properties. FFV values of both the precursors and thermally treated films were estimated from the measured density data using eqn (1), and the results are tabulated in Table 2. For simplicity, since the thermal degradation during the thermal treatment is not significant (<4.5%), the FFV values of the polymers converted at high temperatures with higher than theoretical weight loss were calculated by assuming complete PBO conversion and neglecting thermal degradation. Generally, the FFV increased with increasing the treatment temperature, and all converted films showed higher FFV values than their precursors. For instance, the FFV of TPHI-TR-450 is about 20% higher than that of the TPHI precursor, and an 11.7% increase in FFV was observed for TPHA-TC-400 when compared with the TPHA precursor. The increased FFV in the converted films is mainly because that the conversion to PBO structures greatly disrupted the strong inter-chain interactions (hydrogen-bonding in TPHA and charge-transfer-complex in TPHI) originally present in the precursors leading to an increased inter-chain distance. Comparisons between the TPHI-TR and TPHA-TC series suggested that TR process is likely more efficient in disrupting chain packing and generating free volume than the TC process. In particular, starting from almost the same FFV of ∼17% in the precursors, the FFV values of treated TPHI-TR films are generally higher than those of TPHA-TC counterparts, even though the TPHI-TR films have generally low PBO conversions for given temperature treatment. The difference can be ascribed to the different PBO formation mechanisms associated with these two routes.[16,21] In the TR process, the

hydroxyl groups can react with either of the adjacent carbonyl groups on the imide ring, resulting in a mixture of para- and meta-linked PBOs; however, only para-linked PBOs can be obtained from the cyclodehydration process as there is only one adjacent carbonyl group available to react with the hydroxyl groups in the amide precursor structure. In this regard, a more disrupted chain packing and higher FFV are reasonably expected for TPHI-TR films since the TR process involves more significant changes in chain conformation by transforming heterocyclic imide ring structures to benzoxazole rings. It is also observed that the FFV of TPHA-TC films continued to increase with the cyclodehydration temperature even when full PBO conversion was achieved at 300 °C. This phenomenon is possibly due to the increased tendency of thermal inter-chain cross-linking in the films when treated at a higher temperature, which constrained the chain relaxation preventing collapse of microcavities and more efficiently disrupted chain packing of PBOs resulting in a higher FFV.[54]

Wide angle X-ray diffraction (WAXD) measurements were conducted to examine polymer chain packing for both the precursors and the thermally treated films in the form of inter-chain d-spacing data, which are closely related to FFV and gas transport properties. The WAXD patterns are shown in Fig. 4 and the calculated d-spacing values are listed in Table 2. In general, broad peaks were observed in all WAXD patterns, suggesting amorphous structures of these PBO-based polymers. As expected, the d-spacing value increases with increasing conversion temperature for both series, confirming that a more rigid PBO backbone inhibited tight chain packing resulting in a larger average inter-chain distance. The results are consistent with the trend of FFV as a function of conversion temperature. Comparisons between the samples across the two thermal processes showed that both the absolute d-spacing values as well as the relative increase in d-spacing upon full conversion are higher in the TPHI-TR series than those of the TPHA-TC

Table 2 Density, fractional free volume (FFV), WAXD peak positions (2θ), calculated d-spacing values and mechanical properties of TPHI-TR and TPHA-TC films treated at different temperatures compared with relevant polymers reported previously

	Density (g cm^{-1})	FFV (%)	2θ (°)	d-Spacing (Å)	Elastic modulus (GPa)	Tensile strength (MPa)	Elongation at break (%)
TPHI precursor	1.339	17.0	13.7	6.5	3.41 ± 0.07	87 ± 12	2.9 ± 0.5
TPHI-TR-350	1.318	18.1	13.3	6.7	3.08 ± 0.26	37 ± 3	1.1 ± 0.1
TPHI-TR-400	1.287	19.6	12.5	7.1	a	a	a
TPHI-TR-450	1.273	20.4	11.8	7.5	a	a	a
TPHA precursor	1.340	17.1	14.7	6.0	3.16 ± 0.09	91 ± 3	3.3 ± 0.2
TPHA-TC-300	1.307	18.3	13.6	6.5	2.60 ± 0.19	96 ± 7	4.9 ± 0.6
TPHA-TC-350	1.298	18.8	13.5	6.6	2.71 ± 0.23	88 ± 16	4.4 ± 0.9
TPHA-TC-400	1.295	19.1	13.0	6.8	2.43 ± 0.30	80 ± 11	4.3 ± 0.8
API-TR-450[16]	1.434	20.6	14.5	6.1	—	—	—
PHA-PBO-350[16]	1.402	22.3	15.0	5.9	—	—	—
HAB-6FDA-TR450[55]	1.343	19.5	—	—	2.52	62	2.9
SpiroTR-PBO-6F[51]	1.12	27	13.8	6.4	—	82.3	20
B-TR-PBOIb-1h[15]	1.437	17.7	—	5.98	1.59 ± 0.19	114 ± 12	13.4 ± 3.0
TR-PBO-co-I-3-BAPP[56]	1.360	17.0	—	—	—	111	21.6
Polysulfone[57]	—	14.4	—	—	2.00	54.2	48
Matrimid® 5218[58]	—	17.0	—	—	2.41	87.1	21.1

a Samples were too brittle for measuring tensile properties.

This journal is © The Royal Society of Chemistry 2016

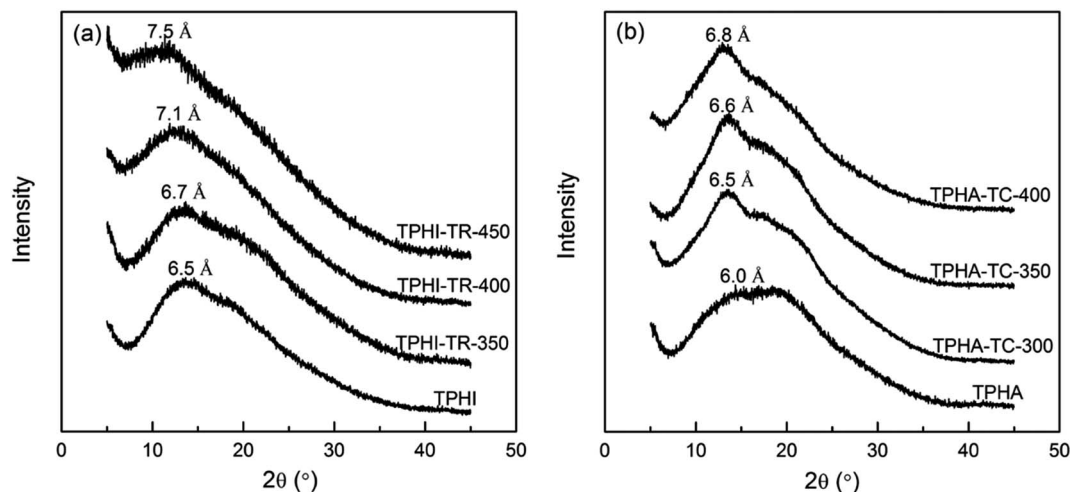*J. Mater. Chem. A*, 2016, **4**, 17050–17062 | **17057**

Fig. 4 WAXD patterns of the (a) TPHI precursor and TPHI-TR films converted at different temperatures, and (b) TPHA precursor and converted TPHA-TC films.

series obtained from the cyclodehydration process, indicating that more significant changes in chain packing occurred in the TR process. Compared with previously reported non-triptycene-containing 6FDA-6FAP-based API-TR-450 and 6FC-6FAP-based PHA-PBO-350 films,[16] the *d*-spacing values of the fully converted TPHI-TR-450 and TPHA-TC-400 films are much higher, indicating that bulky triptycene units synergistically contributed to the effective disruption of tight chain packing in these thermally converted films.

TR polymers prepared at high conversion temperatures are often brittle and fragile most likely due to thermal degradation,[20,55] which represents a technical challenge in the commercialization of TR polymers for gas separations despite their superior gas separation performance. On the other hand, thermal cyclodehydration of poly(hydroxyamide) precursors takes place at a relatively lower temperature, which may produce tougher and more robust polymers with comparable gas transport properties.[16] Mechanical properties of both TPHI and TPHA precursors and converted polymer thin films (Fig. S2†) were evaluated in uniaxial tension and reported as the elastic modulus, tensile strength and elongation at break (Table 2). The mechanical properties of TPHI-TR films are clearly deteriorated from the TPHI precursor. For example, both the tensile strength and the elongation at break of the TPHI-TR-350 film are around 60% lower than those of the TPHI precursor, along with ∼10% decrease in the elastic modulus. Mechanical properties of TPHI-TR polymers prepared at high temperatures (*i.e.*, 400 and 450 °C) were not able to be measured in uniaxial tension due to the brittleness of these samples. The deterioration of mechanical properties during the TR process is likely due to the high rigidity of PBO structures relative to the polyimide precursor, which increases the brittleness of the polymers. Additionally, TR reactions at high temperatures (400–450 °C) are likely accompanied by undesired thermal degradation due to approaching the thermal degradation temperature of the TPHI precursor, leading to dramatically deteriorated mechanical properties in TPHI-TR polymers. In contrast, the TPHA-TC polymers exhibited

mechanical properties comparable to those of the TPHA precursor, from which they were prepared *via* thermal cyclodehydration. All TPHA-TC films are stronger and more ductile than the corresponding TPHI-TR samples despite sharing similar PBO-based structures. In particular, the tensile strength and the elongation at break of TPHA-TC-300 are slightly higher than those of the TPHA precursor, possibly due to the amide-to-benzoxazole structural transformation upon thermal cyclodehydration. The small decrease in tensile strength and elongation at break with increasing cyclodehydration temperature is likely due to thermal degradation, but is much less significant compared with that in the TR process.

The elastic modulus and tensile strength of both TPHI and TPHA precursors are comparable to or greater than those reported for some commercial gas separation polymers, such as Matrimid® polyimide and polysulfone (Table 2).[57,58] However, TPHI and TPHA precursors are less ductile, possibly due to more rigid backbone structures and lower molecular weight. Compared to other reported PBOs with comparable structures,[20,55] the triptycene-containing TPHA-TC series exhibited improved mechanical properties, suggesting that triptycene units are instrumental in strengthening and toughening the PBO polymers and cyclodehydration is a more viable approach to produce robust PBO-based polymers than TR process. Some recent studies showed that the ductility and/or tensile strength of PBO-based polymers derived from the TR process could be improved *via* either copolymerization with non-rearrangable polyimides[15,56] (*e.g.*, PBO-PI copolymers), or introduction of spiro-centers to induce polymer chain entanglement.[51] However, several factors other than the polymer backbone chemical structure, such as the molecular weight of the precursor and thermal treatment protocol (*i.e.*, heating and cooling rate, duration, *etc.*), also play important roles in determining the mechanical properties of the resulting PBO-based polymers. Therefore, the respective contributions of these factors on the overall mechanical properties are difficult to isolate.

3.4. Gas transport properties of precursor films and TPHI-TR and TPHA-TC films

Pure gas transport properties of both precursors and converted PBO-based polymers were tested with four gases (*i.e.*, H_2, CO_2, CH_4 and N_2) using the constant-volume/variable-pressure method.[41] The upstream pressure was varied in a wide range from ~4 to 15 atm to study the feed pressure dependence of gas permeability and possible plasticization behavior. Previous studies have demonstrated that fully converted TR membranes exhibited excellent resistance to CO_2-induced plasticization in mixed-gas permeation experiments for CO_2 partial pressure as high as 25 atm.[11,59,60] As shown in Fig. S3,† no significant plasticization behavior was observed for both TR and TC films in these pure gas permeation studies; a very weak dependence of permeability on the feed pressure was observed, and CO_2 permeabilities exhibited no significant variation with upstream pressure up to 15 atm. Gas transport properties at 11 atm and 35 °C are summarized in Table 3 in terms of permeability and ideal selectivity.

Generally, gas permeabilities for all of the polymers follow the reverse order of kinetic diameter of penetrant molecules, *i.e.*, $H_2 > CO_2 > N_2 > CH_4$, suggesting that diffusivity plays a dominant role in the gas permeation in these polymers. Gas permeabilities of the TPHI precursor are very close to those of the TPHA precursor for all the test gases, which is consistent with the observation that they have almost the same fractional free volume (~17%). Upon thermal conversion to PBO-based structures, the permeabilities of both TPHI-TR and TPHA-TC polymers increase significantly with increasing degree of PBO conversion (or thermal treatment temperature). The trends correspond well with FFV and WAXD results, indicating the formation of a microporous structure during the thermally induced structural transformations to benzoxazoles. Compared with the thermal cyclodehydration process of the TPHA precursor, the increase in gas permeabilities is much more

significant for the TPHI thermal rearrangement route (Fig. 5). For example, the TPHI-TR-450 film exhibits an around 30 times increase in H_2 permeability from the TPHI precursor, while the TPHA-TC-400 film shows a more than two times increase in H_2 permeability, although both films are considered to have fully converted benzoxazole structures. The difference in gas permeabilities of the resulting PBO-based polymers can be ascribed to the different structural transformation mechanisms: the TR process of the TPHI precursor involves complicated rearrangements of heterocyclic ring structures and forms mixed PBO structures of both *meta*- and *para*-linkages with markedly increased chain tortuosity; while the conformational change during the cyclodehydration of the TPHA precursor propagates relatively linearly along the backbone structure leading to less significant chain contortions. Although the TPHA precursor was fully converted to PBO at 300 °C, the slight increase of gas permeabilities in TPHA-350 and TPHA-400 compared to TPHA-300 can be ascribed to the marginal thermal degradation of PBOs at higher thermal treatment temperatures (Table 1).

Surprisingly, the TPHI-TR-450 film showed lower permeabilities than the TPHI-TR-400 film for large gases like CO_2, N_2 and CH_4 (Fig. 5a). Based on the observation that H_2 permeability of the TPHI-TR-450 film is still significantly higher (55% higher) than that of the TPHI-TR-400 film, it seems to suggest that thermal rearrangement of TPHI at high temperatures (>400 °C) generates a large amount of ultra-fine microcavities, which was demonstrated by PALS (positron annihilation lifetime spectroscopy) results in our previous studies.[27,32] This ultrafine microporosity allows fast permeation of H_2 while hindering the permeation of larger gases (CO_2, N_2 and CH_4). As a result, high selectivities of hydrogen-related gas pairs were largely recovered in the TPHI-TR-450 film along with a huge increase in H_2 permeability. These ultrafine microcavities might include both the (partially occupied) internal free volume of

Table 3 Pure gas permeabilities (P) and ideal selectivities (α) of TPHI-TR and TPHA-TC polymers at 11 atm and 35 °C

Polymer	Permeability (barrer)				Ideal selectivity (α)			
	H_2	CO_2	N_2	CH_4	H_2/N_2	H_2/CH_4	CO_2/N_2	CO_2/CH_4
TPHI precursor[27]	27	4.7	0.19	0.09	140	300	25	52
TPHI-TR-350	61	16	0.46	0.41	130	150	35	39
TPHI-TR-400	520	320	16	8.3	32	62	20	39
TPHI-TR-450	810	270	8.4	4.0	96	200	32	67
TPHA precursor	27	5.7	0.21	0.12	130	220	27	48
TPHA-TC-300	74	23	1.1	0.82	67	90	21	28
TPHA-TC-350	82	31	1.4	1.3	59	66	22	24
TPHA-TC-400	92	39	2.2	1.7	42	54	18	23
6FAP-6FDA-450[16]	880	780	59	37	15	24	13	21
6FAP-6FC-350[16]	233	140	9.0	5.2	26	45	16	27
PEBO-450-3[20]	439	486	20	17	22	26	24	29
R-TR-PBOIb-2h[15]	135	66	2.6	1.2	52	113	25	55
TR-PBO-co-I-DAM[56]	53	24	0.79	0.43	67	123	30	56
XTR-PBOI-15[61]	553	655	29.2	19.8	19	28	22	33
XTR-PBOI-5[62]	603	746	29.6	19.9				
Matrimid®[58]	17.5	7.29	0.22	0.21	80	83	33	35
Polysulfone[63]	14	5.6	0.25	0.25	56	56	22	22

This journal is © The Royal Society of Chemistry 2016

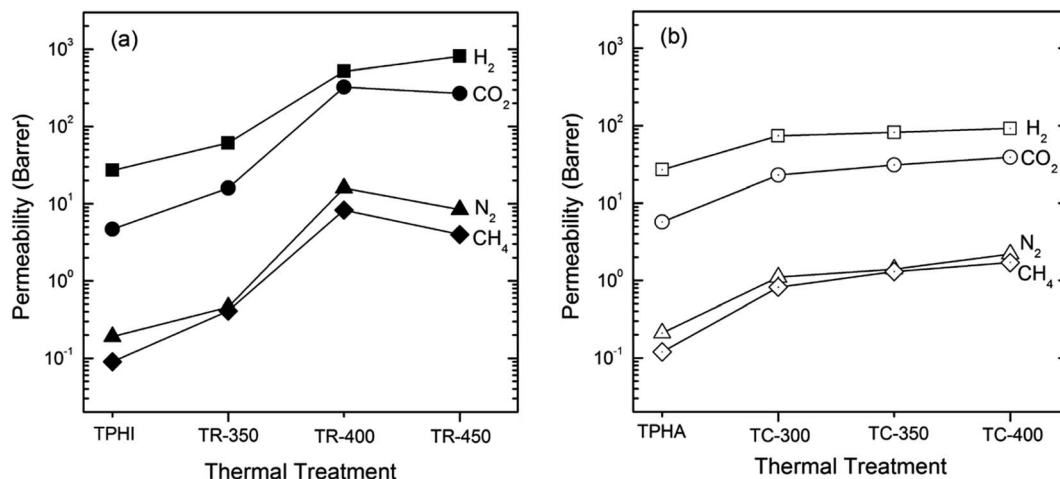*J. Mater. Chem. A*, 2016, **4**, 17050–17062 | **17059**

Fig. 5 Gas permeabilities as a function of thermal treatment temperature for the (a) TPHI-TR series and (b) TPHA-TC series of polymers.

triptycene units and those possibly collapsed from large microcavities at high temperatures, which act as interconnections between larger microcavities and afford high permeability for small gas molecules such as H_2, but not for larger molecules such as N_2 and CH_4, leading to high H_2/N_2 and H_2/CH_4 selectivities. Similar enhancement of gas selectivities by triptycene units was also observed in other reported triptycene-containing PIMs (*e.g.*, TPIM-1, KAUST-PI-1 and PIM-Trip-TB), in which the ultra-microporosity fine-tuned by introducing triptycene building blocks overcame the low selectivities of standard PIMs leading to superior performance for hydrogen purification and air separation membranes.[9,10,31,64]

The overall gas transport properties of both the TPHI-TR and TPHA-TC series of polymers were further summarized in the Robeson's permeability–selectivity tradeoff plots for CO_2/CH_4, H_2/N_2 and H_2/CH_4 gas pairs, shown in Fig. 6. Relevant commercial membrane polymers, *i.e.*, Matrimid® polyimide and polysulfone, and previously reported non-triptycene-containing PBO-based polymers, *e.g.*, TR-PBOs with ether linages, PBO-polyimide copolymers and cross-linked TR membranes,

are also included in these plots for comparisons. As a general trend, TR conversion of the TPHI precursor to PBOs significantly improved gas separation performance by progressively moving both permeability and selectivity towards and eventually beyond the upper bounds. In particular, the TPHI-TR-450 film showed ultrafast and selective CO_2 and H_2 permeation, which placed its separation performance far beyond the 2008 upper bounds for CO_2/CH_4, H_2/N_2 and H_2/CH_4 gas pairs due to the formation of ultrafine microcavities during the TR process discussed before. This synergetic improvement in both permeability and selectivity has been rarely observed for other non-triptycene-containing TR polymers, which typically suffered significant losses in selectivities despite significant gains in permeabilities.[13,16,21] Compared with the most studied TR-450 polymer fabricated from the 6FDA-6FAP poly(hydroxyimide) precursor[16,21] and recently studied PBOs bearing ether linages[20] or PBO-polyimide copolymers,[15,18,56] the triptycene-containing TPHI-TR-450 film has significantly higher selectivities and very comparable permeabilities. Additionally, Lee *et al.* recently constituted a novel methodology to fabricate cross-linked
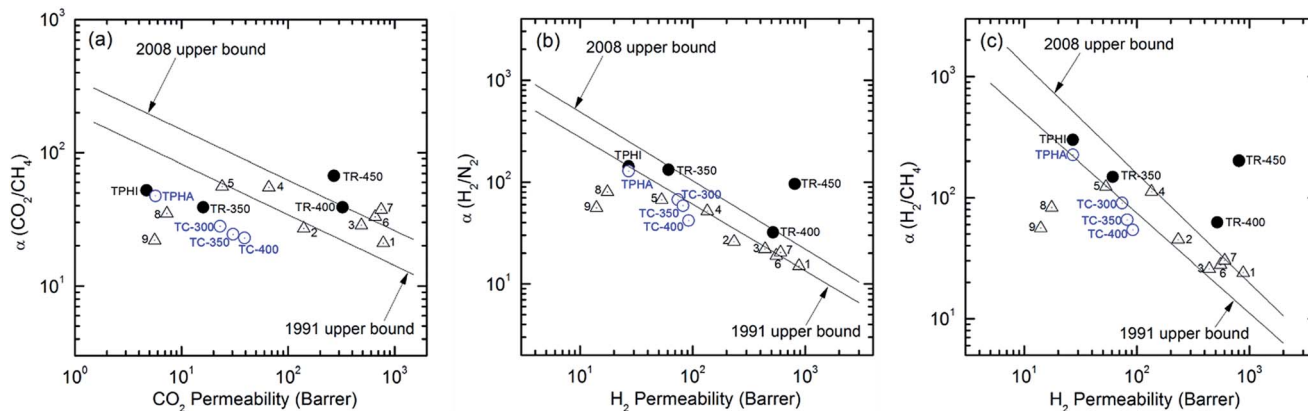

Fig. 6 Permeability–selectivity upper bound plots of TPHI-TR (●) and TPHA-TC (○) polymers for (a) CO_2/CH_4, (b) H_2/N_2 and (c) H_2/CH_4 gas pairs. Other comparative data points are included: 6FAP-6FDA-450 (1),[16] 6F-based PHA-PBO-350 (2),[16] PEBO-450-3 (3),[20] R-TR-PBOIb-2h (4),[15] TR-PBO-*co*-I-DAM (5),[56] XTR-PBOI-15 (6),[61] XTR-PBOI-5 (7),[62] Matrimid® (8),[58] and polysulfone (9).[63]

TR-PBO membranes, which not only enhanced gas permeability and selectivity, but also provided excellent resistance to plasticization up to 40 bar for CO_2/CH_4 separation.[61,62] TPHI-TR-400 and TPHI-TR-450 films exhibit very comparable gas permeabilities and higher gas selectivities compared with these cross-linked TR-PBOs, as shown in Fig. 6. The comparison results seem to indicate that the incorporation of triptycene units into TR polymers helps to optimize the microcavity architecture that greatly promotes molecular sieving properties of TR polymers.

For the TPHA-TC series, the marked increase in gas permeabilities with increasing cyclodehydration temperature or PBO conversion, was, however, accompanied by obvious loss in gas selectivities, which failed to advance the overall gas separation performance of TPHA-TC polymers beyond the upper bounds. However, TPHA-TC polymers still significantly outperformed commercial gas separation polymers (e.g., Matrimid® and polysulfone). Comparisons between TPHA-TC polymers with previously reported PHA-PBO polymers prepared from non-iptycene-containing 6FAP-6FC poly(hydroxyamide) precursor[16] lead to the same conclusion that triptycene structure is instrumental in constructing well-defined microporous architecture facilitating highly selective H_2 transport via size sieving. As shown in Fig. 6, given the same thermal cyclodehydration temperature, the TPHA-TC-350 film in this study shows much higher H_2 selectivities than the corresponding 6F-based PHA-PBO-350 film. Although the separation performance of TPHA-TC polymers is not as superb as that of corresponding TPHI-TR polymers, it should be mentioned that mechanical properties are much better for TPHA-TC polymers, which is critical for practical implementation of these new PBO-based polymers for gas separation applications.

4. Conclusions

Novel triptycene-containing PBO-based films demonstrating excellent gas separation performance were prepared from triptycene-containing polyimide and polyamide precursors with an ortho-hydroxy functionality. Gravimetric and structural analyses indicated that conversion of the TPHA precursor to the PBO structure via the thermal cyclodehydration (TC) process proceeds more readily than the TR process of the TPHI precursor. In particular, full PBO conversion was achieved at 300 °C in the TC process, which is at least 100 °C lower than that in the TR process. The higher TR conversion temperature of TPHI is possibly due to the higher activation energy of the imide-to-benzoxazole conversion. Relatively lower conversion temperature for the TC process also led to significantly better mechanical properties of fully converted TPHA-TC films than those of TPHI-TR films and other reported non-triptycene-containing PBO-based polymers due to a much lower level of thermal degradation. The d-spacing and fractional free volume values of the thermally converted films via both routes increased with increasing thermal treatment temperature. High temperature conversion led to deteriorated mechanical properties for the TPHI-TR films; however, the TPHA-TC films exhibited mechanical properties superior to many other reported TR polymers. Dramatic improvements in gas

permeabilities were achieved upon thermal conversion of the TPHI precursor to PBOs, and the high selectivities were not affected. In particular, TPHI-TR-400 and TPHI-TR-450 polymers showed superb separation performance for CO_2/CH_4, H_2/N_2 and H_2/CH_4 gas pairs that exceeded the 2008 upper bounds. TPHA-TC films exhibited less significant improvement of gas separation performance, probably due to less significant changes in chain conformation during thermal conversion.

Acknowledgements

References

1 R. W. Baker and B. T. Low, Macromolecules, 2014, 47, 6999–7013.

2 Y. Yampolskii, Macromolecules, 2012, 45, 3298–3311.

3 D. F. Sanders, Z. P. Smith, R. Guo, L. M. Robeson, J. E. McGrath, D. R. Paul and B. D. Freeman, Polymer, 2013, 54, 4729–4761.

4 L. M. Robeson, J. Membr. Sci., 1991, 62, 165–185.

5 L. M. Robeson, J. Membr. Sci., 2008, 320, 390–400.

6 M. D. Guiver and Y. M. Lee, Science, 2013, 339, 284–285.

7 N. B. McKeown and P. M. Budd, Chem. Soc. Rev., 2006, 35, 675–683.

8 N. Du, H. B. Park, G. P. Robertson, M. M. Dal-Cin, T. Visser, L. Scoles and M. D. Guiver, Nat. Mater., 2011, 10, 372–375.

9 B. S. Ghanem, R. Swaidan, E. Litwiller and I. Pinnau, Adv. Mater., 2014, 26, 3688–3692.

10 M. Carta, M. Croad, R. Malpass-Evans, J. C. Jansen, P. Bernardo, G. Clarizia, K. Friess, M. Lanc and N. B. McKeown, Adv. Mater., 2014, 26, 3526–3531.

11 H. B. Park, C. H. Jung, Y. M. Lee, A. J. Hill, S. J. Pas, S. T. Mudie, E. Van Wagner, B. D. Freeman and D. J. Cookson, Science, 2007, 318, 254–258.

12 S. Kim and Y. M. Lee, Prog. Polym. Sci., 2015, 43, 1–32.

13 R. Guo, D. F. Sanders, Z. P. Smith, B. D. Freeman, D. R. Paul and J. E. McGrath, J. Mater. Chem. A, 2013, 1, 6063–6072.

14 R. Guo, D. F. Sanders, Z. P. Smith, B. D. Freeman, D. R. Paul and J. E. McGrath, J. Mater. Chem. A, 2013, 1, 262–272.

15 Y. Zhuang, J. G. Seong, W. H. Lee, Y. S. Do, M. J. Lee, G. Wang, M. D. Guiver and Y. M. Lee, Macromolecules, 2015, 48, 5286–5299.

16 A. Kushwaha, M. E. Dose, Z. P. Smith, S. Luo, B. D. Freeman and R. Guo, Polymer, 2015, 78, 81–93.

17 Y. Jiang, F. T. Willmore, D. Sanders, Z. P. Smith, C. P. Ribeiro, C. M. Doherty, A. Thornton, A. J. Hill, B. D. Freeman and I. C. Sanchez, Polymer, 2011, 52, 2244–2254.

18 C. H. Jung, J. E. Lee, S. H. Han, H. B. Park and Y. M. Lee, *J. Membr. Sci.*, 2010, **350**, 301–309.

19 J. I. Choi, C. H. Jung, S. H. Han, H. B. Park and Y. M. Lee, *J. Membr. Sci.*, 2010, **349**, 358–368.

20 M. Calle and Y. M. Lee, *Macromolecules*, 2011, **44**, 1156–1165.

21 Z. P. Smith, K. Czenkusch, S. Wi, K. L. Gleason, G. Hernandez, C. M. Doherty, K. Konstas, T. J. Bastow, C. Alvarez, A. J. Hill, A. E. Lozano, D. R. Paul and B. D. Freeman, *Polymer*, 2014, **55**, 6649–6657.

22 H. Wang and T.-S. Chung, *J. Membr. Sci.*, 2011, **385**, 86–95.

23 H. Wang, S. Liu, T.-S. Chung, H. Chen, Y.-C. Jean and K. P. Pramoda, *Polymer*, 2011, **52**, 5127–5138.

24 S. H. Han, H. J. Kwon, K. Y. Kim, J. G. Seong, C. H. Park, S. Kim, C. M. Doherty, A. W. Thornton, A. J. Hill, A. E. Lozano, K. A. Berchtoldf and Y. M. Lee, *Phys. Chem. Chem. Phys.*, 2012, **14**, 4365–4373.

25 S. Luo, K. A. Stevens, J. S. Park, J. D. Moon, Q. Liu, B. D. Freeman and R. Guo, *ACS Appl. Mater. Interfaces*, 2016, **8**, 2306–2317.

26 S. Luo, Q. Liu, B. Zhang, J. R. Wiegand, B. D. Freeman and R. Guo, *J. Membr. Sci.*, 2015, **480**, 20–30.

27 S. Luo, J. R. Wiegand, B. Kazanowska, C. M. Doherty, K. Konstas, A. J. Hill and R. Guo, *Macromolecules*, 2016, **49**, 3395–3405.

28 J. R. Wiegand, Z. P. Smith, Q. Liu, C. T. Patterson, B. D. Freeman and R. Guo, *J. Mater. Chem. A*, 2014, **2**, 13309–13320.

29 Y. J. Cho and H. B. Park, *Macromol. Rapid Commun.*, 2011, **32**, 579–586.

30 R. Swaidan, M. Al-Saeedi, B. Ghanem, E. Litwiller and I. Pinnau, *Macromolecules*, 2014, **47**, 5104–5114.

31 B. S. Ghanem, R. Swaidan, X. Ma, E. Litwiller and I. Pinnau, *Adv. Mater.*, 2014, **26**, 6696–6700.

32 S. Luo, J. R. Wiegand, P. Gao, C. M. Doherty, A. J. Hill and R. Guo, *J. Membr. Sci.*, 2016, **518**, 100–109.

33 T. M. Swager, *Acc. Chem. Res.*, 2008, **41**, 1181–1189.

34 Y. Jiang and C.-F. Chen, *Eur. J. Org. Chem.*, 2011, 6377–6403.

35 S.-H. Hsiao, H.-M. Wang, W.-J. Chen, T.-M. Lee and C.-M. Leu, *J. Polym. Sci., Part A: Polym. Chem.*, 2011, **49**, 3109–3120.

36 Y. Maruyama, Y. Oishi, M. Kakimoto and Y. Imai, *Macromolecules*, 1988, **21**, 2305–2309.

37 Y. Oishi, A. Konno, J. Oravec and K. Mori, *J. Photopolym. Sci. Technol.*, 2006, **19**, 669–672.

38 ASTM D882-12, *Standard Test Method for Tensile Properties of Thin Plastic Sheeting*, ASTM International, West Conshohocken, PA, 2012.

39 A. Bondi, *J. Phys. Chem.*, 1964, **68**, 441–451.

40 J. Y. Park and D. R. Paul, *J. Membr. Sci.*, 1997, **125**, 23–39.

41 H. Lin and B. D. Freeman, in *Springer Handbook of Material Measurement Methods*, ed. H. Czichos, T. Saito and L. Smith, Springer, New York, 2006, pp. 371–387.

42 M. Calle, Y. Chan, H. J. Jo and Y. M. Lee, *Polymer*, 2012, **53**, 2783–2791.

43 G. L. Tullos, J. M. Powers, S. J. Jeskey and L. J. Mathias, *Macromolecules*, 1999, **32**, 3598–3612.

44 D. Likhatchev, C. GutierrezWing, I. Kardash and R. VeraGraziano, *J. Appl. Polym. Sci.*, 1996, **59**, 725–735.

45 D. Guzman-Lucero and D. Likhatchev, *Polym. Bull.*, 2002, **48**, 261–269.

46 C. H. Park, E. Tocci, Y. M. Lee and E. Drioli, *J. Phys. Chem. B*, 2012, **116**, 12864–12877.

47 H. B. Park, S. H. Han, C. H. Jung, Y. M. Lee and A. J. Hill, *J. Membr. Sci.*, 2010, **359**, 11–24.

48 Z. P. Smith, D. F. Sanders, C. P. Ribeiro, R. Guo, B. D. Freeman, D. R. Paul, J. E. McGrath and S. Swinnea, *J. Membr. Sci.*, 2012, **415**, 558–567.

49 M. Calle, A. E. Lozano and Y. M. Lee, *Eur. Polym. J.*, 2012, **48**, 1313–1322.

50 S. H. Han, N. Misdan, S. Kim, C. M. Doherty, A. J. Hill and Y. M. Lee, *Macromolecules*, 2010, **43**, 7657–7667.

51 S. Li, H. J. Jo, S. H. Han, C. H. Park, S. Kim, P. M. Budd and Y. M. Lee, *J. Membr. Sci.*, 2013, **434**, 137–147.

52 D. F. Sanders, R. L. Guo, Z. P. Smith, Q. Liu, K. A. Stevens, J. E. McGrath, D. R. Paul and B. D. Freeman, *Polymer*, 2014, **55**, 1636–1647.

53 Y. S. Do, J. G. Seong, S. Kim, J. G. Lee and Y. M. Lee, *J. Membr. Sci.*, 2013, **446**, 294–302.

54 W. Qiu, C.-C. Chen, L. Xu, L. Cui, D. R. Paul and W. J. Koros, *Macromolecules*, 2011, **44**, 6046–6056.

55 Q. Liu, D. R. Paul and B. D. Freeman, *Polymer*, 2016, **82**, 378–391.

56 C. Y. Soo, H. J. Jo, Y. M. Lee, J. R. Quay and M. K. Murphy, *J. Membr. Sci.*, 2013, **444**, 365–377.

57 G. S. Sur, H. L. Sun, S. G. Lyu and J. E. Mark, *Polymer*, 2001, **42**, 9783–9789.

58 Y. Zhang, I. H. Musseman, J. P. Ferraris and K. J. Balkus Jr, *J. Membr. Sci.*, 2008, **313**, 170–181.

59 R. Swaidan, X. H. Ma, E. Litwiller and I. Pinnau, *J. Membr. Sci.*, 2013, **447**, 387–394.

60 K. L. Gleason, Z. P. Smith, Q. Liu, D. R. Paul and B. D. Freeman, *J. Membr. Sci.*, 2015, **475**, 204–214.

61 M. Calle, H. J. Jo, C. M. Doherty, A. J. Hill and Y. M. Lee, *Macromolecules*, 2015, **48**, 2603–2613.

62 M. Calle, C. M. Doherty, A. J. Hill and Y. M. Lee, *Macromolecules*, 2013, **46**, 8179–8189.

63 C. L. Aitken, W. J. Koros and D. R. Paul, *Macromolecules*, 1992, **25**, 3424–3434.

64 R. Swaidan, B. Ghanem and I. Pinnau, *ACS Macro Lett.*, 2015, **4**, 947–951.

65 D. F. Sanders, Z. P. Smith, C. P. Ribeiro Jr, R. Guo, J. E. McGrath, D. R. Paul and B. D. Freeman, *J. Membr. Sci.*, 2012, **409**, 232–241.